EPJ Appl. Metamat. **9**, 8 (2022)

https://doi.org/10.1051/epjam/2022005

EPJ Applied Metamaterials

Available online at:
epjam.edp-open.org

Metamaterials for Novel Wave Phenomena in Microwaves, Optics, and Mechanics

RESEARCH ARTICLE OPEN ACCESS

High-sensitivity in various gyrator-based circuits with exceptional points of degeneracy

Kasra Rouhi[1], Alireza Nikzamir[1], Alexander Figotin[2], and Filippo Capolino[1,*]

[1] Department of Electrical Engineering and Computer Science, University of California, Irvine, CA 92697, USA
[2] Department of Mathematics, University of California, Irvine, CA 92697, USA

Received: 13 December 2021 / Accepted: 1 February 2022

Abstract. Exceptional points of degeneracy (EPD) can enhance the sensitivity of circuits by orders of magnitude. We show various configurations of coupled LC resonators via a gyrator that support EPDs of second and third-order. Each resonator includes a capacitor and inductor with a positive or negative value, and the corresponding EPD frequency could be real or imaginary. When a perturbation occurs in the second-order EPD gyrator-based circuit, we show that there are two real-valued frequencies shifted from the EPD one, following a square root law. This is contrary to what happens in a Parity-Time (PT) symmetric circuits where the two perturbed resonances are complex valued. We show how to get a stable EPD by coupling two unstable resonators, how to get an unstable EPD with an imaginary frequency, and how to get an EPD with a real frequency using an asymmetric gyrator. The relevant Puiseux fractional power series expansion shows the EPD occurrence and the circuit's sensitivity to perturbations. Our findings pave the way for new types of high-sensitive devices that can be used to sense physical, chemical, or biological changes.

Keywords: Coupled resonators / enhanced sensitivity / exceptional points of degeneracy (EPDs) / gyrator / perturbation theory

1 Introduction

The presence of at least one nontrivial Jordan block in the Jordan canonical form of the system matrix shows an exceptional point of degeneracy (EPD) [1–4], as was demonstrated in Parity-Time (PT) symmetric systems [5–12]. Analogous concepts were discovered in the area of slow light in propagation in photonic crystals by Figotin and Vitebskiy in [13–16] even though they did not use the term "exceptional point". The strong sensitivity of the degenerate eigenvalues (i.e., degenerate resonance frequencies) to perturbations is a remarkable feature of EPDs [4]. We emphasize the necessity of referring to it as a "degeneracy", hence, incorporating the D in EPD, because the defining feature of an exceptional point is the strong full degeneracy of at least two eigenmodes, as implied in [17]. When a second-order EPD with two coalesced eigenstates is subject to a small perturbation Δ, the eigenvalue splitting is proportional to the square root of Δ, which is larger than the linear splitting of conventional sensors without degeneracy [18]. Moreover, the sensitivity increases by increasing the order of the degeneracy, whereas a more complex system is needed. The physics of operating near an EPD may improve a sensor response to a perturbation by an amount that grows with the proximity of the sensor's operating point to the EPD [10,19,20]. Noise may also play a critical role in the performance of these kinds of sensing applications based on EPD, also depending on the chosen circuit configuration [12]. Although this topic requires further investigation, some discussion can be seen in [21–24]. The concept of EPD has been investigated in lossless, spatially [14,25,26] or temporally [27,28] periodic structures and in circuits with loss and/or gain under parity-time symmetry [29–31]. The EPD-based principle of higher sensitivity has been proposed in various sensing systems, including optical microcavities [32], electron beam devices [33,34], optomechanical mass sensors [35], and ring laser gyroscopes [36].

Previously, most of the published EPDs circuits were based on coupled resonators with gain and loss, satisfying PT-symmetry [5–12]. This paper shows and discusses a new way developed at UC Irvine to obtain EPDs based on coupling LC circuits by gyrators. A gyrator is a two-port and nonreciprocal component invented by Tellegen in 1948 and proposed as a fifth fundamental network element,

* e-mail: f.capolino@uci.edu

alongside the resistor, capacitor, inductor, and transformer [37]. Numerous publications on the development and deployment of the gyrator have been written since its invention. Gyrators have been designed using vacuum tubes, transistors [38–45], and operational amplifiers (opamps) [46–53] due to their nonreciprocal property. In addition, a brief review of various methods and electronic circuits to realize the gyrator is summarized in Appendix A. In addition, the gyrator concept is not restricted to a two-port network, and it can be extended to various complex models such as the three-port gyrator [54]. A gyrator loaded with a capacitor is used to realize an effective inductance, so passive RLC networks can be synthesized using only resistors, capacitors, and gyrators [50]. Also, RLC filters can be constructed utilizing gyrators without using inductances [50]. More details on important features and specific characteristics of the gyrator are presented in Appendix B.

In this paper, we study various schemes to get EPDs in gyrator-based sensing circuits, as well as their enhanced sensitivity when operating near an EPD. First, two series LC resonators are coupled via a gyrator, as explained in [55–59], leading to a second-order EPD. Next, we extend our study to a third-order EPD obtained using three LC resonators and two gyrators. In this case, the circuit's sensitivity is enhanced, although the circuit is always unstable. The second part of this paper investigates gyrator circuits with parallel LC resonators, a dual version of the series configuration. It covers various cases leading to (i) stable EPDs by coupling two unstable resonators, (ii) EPDs with imaginary frequency, and (iii) EPDs using two LC circuits and an asymmetric gyrator. We show examples for all the cases and analyze the second-order circuits' signal using time-domain simulations. In addition, the sensitivity of circuit eigenfrequencies to component variations is investigated. We demonstrate that the Puiseux fractional power series expansion closely approximates the eigenfrequency diagram bifurcation near the EPD [4]. This paper explores and reviews specific cases, whereas a mathematical framework for constructing lossless circuits for any conceivable Jordan structure using a gyrator has been presented in [55]. In addition, we consider lossless components in our study, and the analysis of stability or instability in some circuit configurations by adding small losses to the circuits is discussed in [57,58]. The analysis and circuit presented in this paper have great potential applications in novel ultra-high-sensitive schemes.

2 EPD in series configuration

This section reviews various series configurations with gyrators to obtain an EPD. We provide the required circuit equations to get the EPD conditions based on a Liouvillian formalism. We build the eigenvalue problem to find a second-order EPD, leading to two resonant frequencies, and demonstrate the condition for obtaining EPD at the desired frequency. Moreover, we show the circuit's perturbation effects on the eigenfrequencies. Besides the theoretical calculations, we also perform time-domain circuit simulations. We estimate the eigenfrequencies by using the Puiseux fractional power series expansion. The first part summarizes the analysis provided in [58] but later is cast in a more general way to include all cases. Next, we demonstrate a third-order EPD in three LC series resonators coupled via two gyrators. In this latter case, the circuit's sensitivity increases dramatically because of the higher EPD order. However, a more complex circuit with more components is needed, and the circuit is unstable.

2.1 Second-order EPD

In the first circuit, shown in Figure 1a, two series LC tanks are connected via an ideal gyrator. All of the components in the circuit are assumed to be ideal, so there is no resistance in the circuit. The Kirchhoff voltage law equations are written in two loops [58]

$$\begin{cases} \ddot{Q}_1 = -\dfrac{1}{C_1 L_1} Q_1 + \dfrac{R_g}{L_1}\dot{Q}_2 \\ \ddot{Q}_2 = -\dfrac{1}{C_2 L_2} Q_2 - \dfrac{R_g}{L_2}\dot{Q}_1 \end{cases}. \tag{1}$$

In the above equations, Q_n is the stored charge in the capacitor C_n, where $n=1$ indicates the left resonator and $n=2$ indicates the right resonator. It is convenient to define a state vector as $\boldsymbol{\Psi} \equiv \left[Q_1, Q_2, \dot{Q}_1, \dot{Q}_2\right]^{\mathrm{T}}$, which consists of a combination of stored charges and their time derivative on both sides, and the superscript T denotes the transpose operation. Finally, we express the equations in Liouvillian form as [58]

$$\frac{\mathrm{d}\boldsymbol{\Psi}}{\mathrm{d}t} = \underline{\mathbf{M}}\boldsymbol{\Psi}, \tag{2}$$

$$\underline{\mathbf{M}} = \begin{bmatrix} 0 & 0 & 1 & 0 \\ 0 & 0 & 0 & 1 \\ -\omega_{01}^2 & 0 & 0 & -\dfrac{R_g}{L_1} \\ 0 & -\omega_{02}^2 & -\dfrac{R_g}{L_2} & 0 \end{bmatrix}. \tag{3}$$

Here, $\omega_{01} = 1/\sqrt{C_1 L_1}$, and $\omega_{02} = 1/\sqrt{C_2 L_2}$ are resonance angular frequencies of two isolated resonators, i.e., without coupling. We will assume that both resonators have a real resonance frequency in this section, so the inductance and capacitance in each resonator have the same sign. Considering signals of the form $Q_n \propto e^{j\omega t}$, where ω is the angular eigenfrequency. We write the eigenvalue problem associated with the circuit equations, and the characteristic equation is obtained from $\det(\underline{\mathbf{M}} - j\omega\,\underline{\mathbf{I}}) = 0$, where $\underline{\mathbf{I}}$ is the identity matrix, leading to [58]

$$\omega^4 - \omega^2\left(\omega_{01}^2 + \omega_{02}^2 + \frac{R_g^2}{L_1 L_2}\right) + \omega_{01}^2\omega_{02}^2 = 0. \tag{4}$$

In the characteristic equation, all the ω's coefficients are real, so both ω and ω^* are roots of the equation, where * represents the complex conjugate operation. In addition, the characteristic equation is quadratic in ω^2; so, ω and $-\omega$

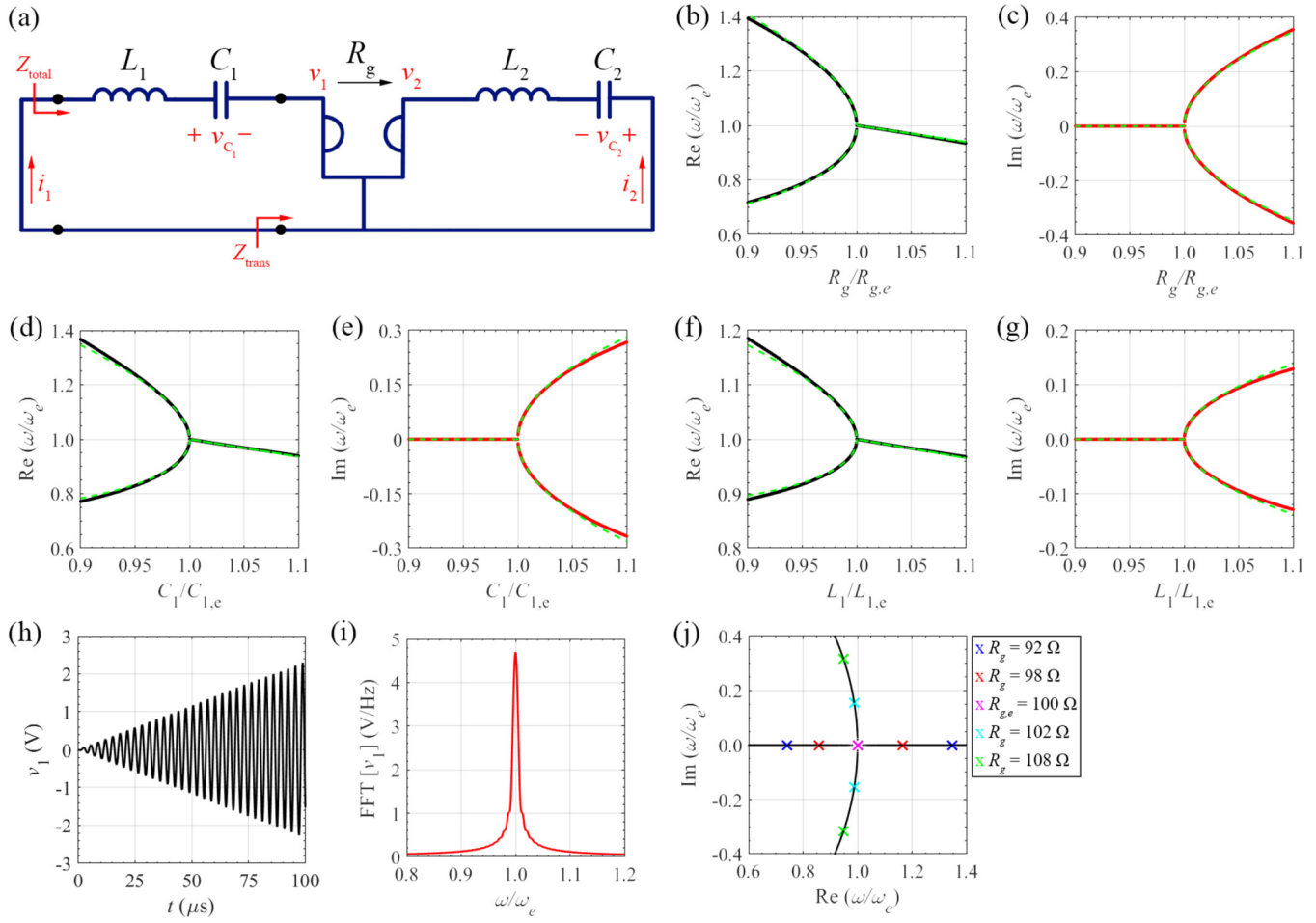

Fig. 1. (a) The schematic illustration of the gyrator-based circuit with the ideal gyrator in series configuration. In this circuit, two different LC resonators are used in a series configuration, coupled via an ideal gyrator. The sensitivity of the (b), (d), (f) real and (c), (e), (g) imaginary parts of the eigenfrequencies to (b), (c) gyration resistance, (d), (e) positive capacitance C_1 (f), (g) positive inductance L_1 perturbation. Solid lines: solution of eigenvalue problem of equation (2); green-dashed lines: Puiseux series approximation truncated to its second term. Voltage $v_1(t)$ under the EPD condition in the (h) time-domain, and (i) frequency-domain. The frequency-domain result is calculated by applying an FFT with 10^6 samples in the time window of 0 µs to 100 µs. (j) Root locus of zeros of $Z_{total}(\omega) = 0$ showing the real and imaginary parts of resonance frequencies of the circuit when perturbing gyration resistance. At the EPD, the system's total impedance is $Z_{total}(\omega) \propto (\omega - \omega_e)^2$; hence it shows a double zero at ω_e.

are both solutions. When $R_g = 0$, the two resonators are uncoupled, and the two independent circuits have two angular eigenfrequency pairs of $\omega_{1,3} = \pm\omega_{01}$, and $\omega_{2,4} = \pm\omega_{02}$. In the gyrator-based circuit, the angular eigenfrequencies are determined as [58]

$$\omega_{1,3} = \pm\sqrt{a+b},\ \omega_{2,4} = \pm\sqrt{a-b}, \tag{5}$$

$$a = \frac{1}{2}\left(\omega_{01}^2 + \omega_{02}^2 + \frac{R_g^2}{L_1 L_2}\right). \tag{6}$$

$$b^2 = a^2 - \omega_{01}^2\omega_{02}^2. \tag{7}$$

Based on equation (5), the EPD can be obtained when $b = 0$ and the corresponding EPD angular frequency is $\omega_e = \sqrt{a}$. Here we consider EPD with real eigenfrequency, so a is a positive value. The condition for real EPD frequency is expressed as [58]

$$\omega_{01}^2 + \omega_{02}^2 - \omega_{gs}^2 > 0, \tag{8}$$

where the equivalent gyrator frequency is defined as $\omega_{gs}^2 = -R_g^2/(L_1 L_2)$ for the series configuration [58]. To obtain an EPD in this configuration using equations (6), and (7) the following equation should be satisfied [58],

$$(\omega_{01} - \omega_{02})^2 = \omega_{gs}^2. \tag{9}$$

First, if ω_{01} and ω_{02} are purely real, the value of either L_1 or L_2 should be negative to have the same sign on both sides of equation (9). Thus, one of the resonators should have a negative inductance to have a pure real ω_{01} or ω_{02}.

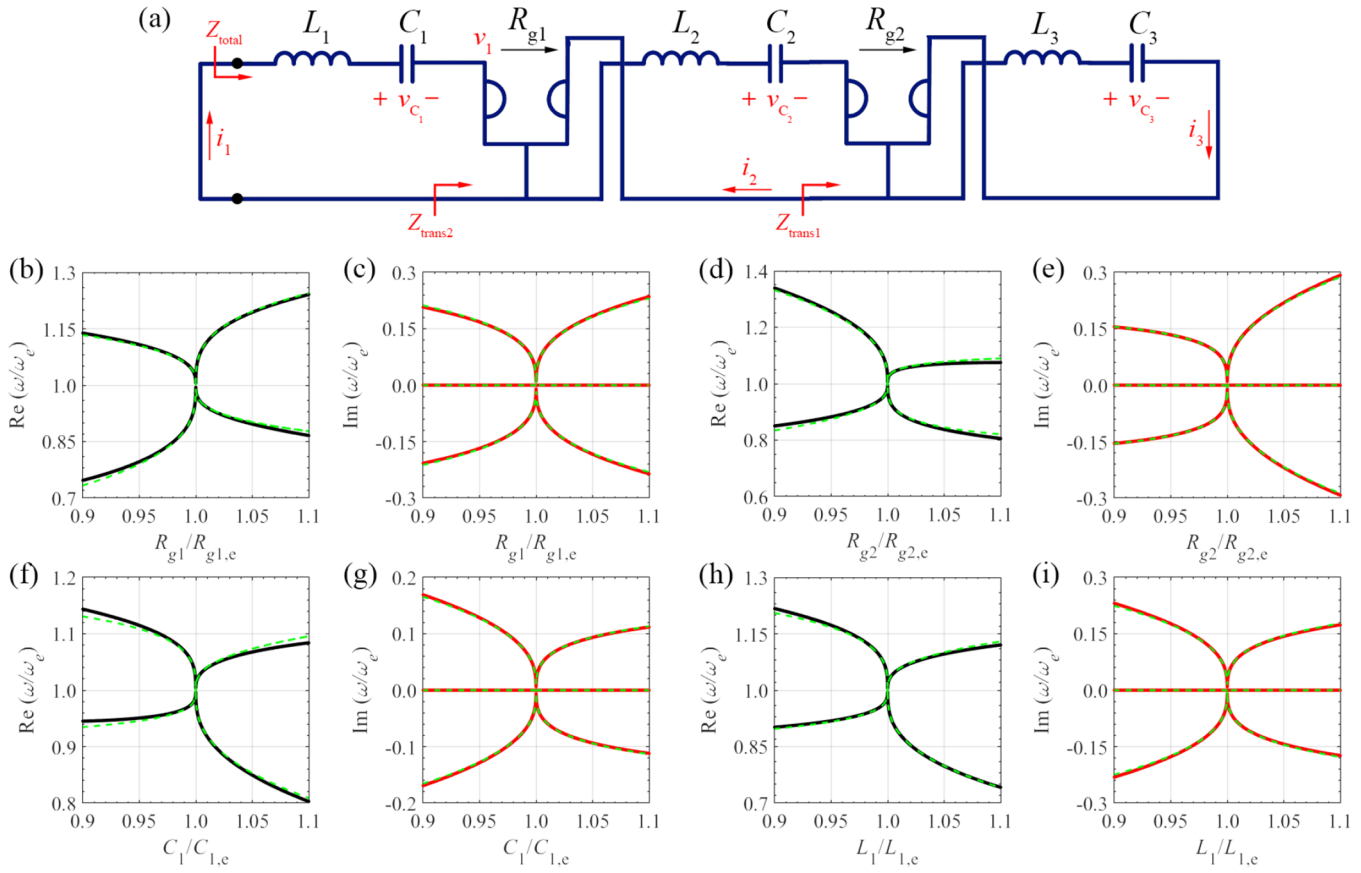

Fig. 2. (a) The schematic illustration of the gyrator-based circuit with the ideal gyrator in third-order configuration. In this circuit, three different LC resonators are coupled via two different ideal gyrators. The sensitivity of the (b), (d), (f), (h) real and (c), (e), (g), (i) imaginary parts of the eigenfrequencies to (b), (c) gyration resistance of the first gyrator R_{g1}, (d), (e) gyration resistance of the second gyrator R_{g2}, (f), (g) positive capacitance C_1 (h), (i) positive inductance L_1 perturbation. Solid lines: solution of eigenvalue problem of equation (14); green-dashed lines: Puiseux series approximation truncated to its second term.

Second, if both ω_{01} and ω_{02} have imaginary values, the selected values for L_1 and L_2 should have the same sign. When L_1 and L_2 are positive, C_1 and C_2 should be negative, or vice versa.

Finally, if only one of the ω_{01} or ω_{02} has imaginary value and the other one has a real value, there are no conditions to obtain an EPD [58]. In this section, we consider the first case in which only one inductor and one capacitor in the same resonator have a negative value so ω_{gs}^2 is positive. The required circuit to synthesize the negative components is described in Appendix C.

The EPD frequency is calculated by using equations (5), (6), and (7) as

$$\omega_e = \sqrt{\frac{1}{2}\left(\omega_{01}^2 + \omega_{02}^2 - \omega_{gs}^2\right)} = \sqrt{\omega_{01}\omega_{02}}. \qquad (10)$$

The EPD condition can be satisfied by many different combinations of component values, and we will use this set of values for components as an example: $L_1 = 33\ \mu\text{H}$, $L_2 = -33\ \mu\text{H}$, $C_2 = -33$ nF, and $R_g = 100\ \Omega$. Then, the capacitance C_1 is determined by solving the quadratic equation from the EPD condition, i.e., $b = 0$. There are two different values of the capacitance C_1 in the first resonator that satisfies the EPD condition, and we select $C_1 = 1.90$ nF for this example. The real and imaginary parts of eigenfrequencies calculated from the eigenvalue problem by perturbing the gyrator resistance R_g near the EPD value of 100 Ω are shown in Figures 1b and 1c. In this example, we have $\omega_e = 1.95 \times 10^6$ rad/s and the calculated eigenvalues are normalized to ω_e. In addition, the calculated results in Figures 1d and 1e show the real and imaginary parts of eigenvalue by perturbing the positive capacitance C_1 in the left resonator. Finally, by changing the positive inductance, the real and imaginary parts of eigenfrequencies are shown in Figures 1f and 1g. To confirm the calculated results and show the sensitivity of the eigenvalues to external perturbation, the eigenfrequencies are also calculated by the Puiseux fractional power series expansion. More details about this method are in Appendix D. The approximated results calculated by the Puiseux series are shown by the green dashed lines in Figures 1b–1g, which show a good agreement with the solutions of the eigenvalue problem in equation (2). In the approximated results, the coefficients of the Puiseux series are calculated as, $\alpha_1 = j2.14 \times 10^6$ rad/s, and $\alpha_2 = -1.17 \times 10^6$ rad/s when perturbing R_g, $\alpha_1 = j1.74 \times 10^6$ rad/s, and $\alpha_2 = -1.26 \times 10^6$ rad/s when perturbing C_1, and $\alpha_1 = j8.52 \times 10^2$ rad/s, and $\alpha_2 = -6.74 \times 10^5$ rad/s when perturbing L_1. The results in Figures 1b–1g

demonstrate that by perturbing R_g, C_1, and L_1, the eigenfrequencies in the gyrator-based circuit always show an analogous behavior. So, by individual variation of the components value, the real parts of the eigenfrequencies split when the value is smaller than the EPD value, and the imaginary parts of the eigenfrequencies split when the value is bigger than the EPD value.

Furthermore, Figures 1h and 1i show the time-domain and frequency-domain simulation results obtained with the Keysight ADS time-domain circuit simulator. The calculated results in these two plots are the voltage $\upsilon_1(t)$ in the left gyrator port and its frequency spectrum, where we use 1 mV as an initial voltage on the left capacitor C_1. According to Figure 1h, the voltage increases linearly, which is an important aspect peculiar to an EPD. This typical signal is the inverse Laplace transform of a double pole, i.e., the result of coalescing circuit eigenvalues and eigenvectors corresponds to a double pole (or a double zero of the total circuit admittance). A linear growth demonstrates a second-order EPD with real frequency in the circuit. We take the fast Fourier transform (FFT) of the voltage $\upsilon_1(t)$ to calculate the frequency spectrum, with 10^6 samples in the time window of 0 µs to 100 µs, and the calculated spectrum is illustrated in Figure 1i. According to the frequency spectrum of the signal, the oscillation angular frequency corresponds to $\omega_e = 1.95 \times 10^6$ rad/s, that is the same as the one obtained from solving the eigenvalue problem. In this example, we used lossless components in the circuit. A complete investigation showing the effect of losses in the series configuration is presented in [58].

The following part demonstrates how the EPD regime is related to a specific type of circuit's resonance, which can be found directly in a frequency-domain analysis of the circuit. The transferred impedance on the left side of the gyrator is expressed as (see Figure 1a)

$$Z_{trans}(\omega) = \frac{R_g^2}{Z_2}. \tag{11}$$

In the above equation, $Z_2(\omega) = j\omega L_2 + 1/(j\omega C_2)$ is the series impedance on the right side of the gyrator. The total impedance observed from the circuit input port (see Figure 1a) is calculated by

$$Z_{total}(\omega) = Z_1(\omega) + Z_{trans}(\omega), \tag{12}$$

where $Z_1(\omega) = j\omega L_1 + 1/(j\omega C_1)$ is the series impedance connected to the left side of the gyrator. The complex-valued resonant frequencies are obtained by imposing $Z_{total}(\omega) = 0$. The real and imaginary parts of calculated resonance frequency by finding the zeros of such total impedance $Z_{total}(\omega)$ for various gyration resistance values are shown in Figure 1j. When the gyration resistance is equal to the corresponding EPD value, the two zeros coincide with the EPD angular frequency ω_e, that is also the point where the two curves in Figure 1j meet where $Z_{total}(\omega) \propto (\omega - \omega_e)^2$. For gyrator resistances such that $R_g < R_{g,e}$, two resonance angular frequencies are purely real. Instead, for $R_g > R_{g,e}$, the two resonance angular frequencies are complex conjugate. In other words, depending on how the circuit is defined, the EPD frequency coincides with double zeros (or double poles, depending on what we look at) of the frequency spectrum.

2.2 Third-order EPD

In this section, we investigate the third-order EPD in the gyrator-based circuit. Three series LC tanks are coupled via two ideal gyrators to obtain third-order EPD, as shown in Figure 2a. We write the Kirchhoff voltage law equations in three loops as

$$\begin{cases} \ddot{Q}_1 = -\dfrac{1}{C_1 L_1} Q_1 + \dfrac{R_{g1}}{L_1} \dot{Q}_2 \\ \ddot{Q}_2 = -\dfrac{1}{C_2 L_2} Q_2 - \dfrac{R_{g1}}{L_2} \dot{Q}_1 + \dfrac{R_{g2}}{L_2} \dot{Q}_3 \\ \ddot{Q}_3 = -\dfrac{1}{C_3 L_3} Q_3 - \dfrac{R_{g2}}{L_3} \dot{Q}_2 \end{cases}. \tag{13}$$

In these equations, Q_n is the stored charge in the capacitor C_n ($n = 1$ for the left resonator, $n = 2$ for the middle resonator, and $n = 3$ for the right resonator). In this circuit, we consider two different values for the gyration resistance of two gyrators. The state vector for the third-order circuit is conveniently defined as $\Psi \equiv \left[Q_1, Q_2, Q_3, \dot{Q}_1, \dot{Q}_2, \dot{Q}_3\right]^{\mathrm{T}}$. Finally, the circuit's equations are written in Liouvillian form as

$$\frac{\mathrm{d}\Psi}{\mathrm{d}t} = \underline{\mathbf{M}}\Psi, \tag{14}$$

$$\underline{\mathbf{M}} = \begin{bmatrix} 0 & 0 & 0 & 1 & 0 & 0 \\ 0 & 0 & 0 & 0 & 1 & 0 \\ 0 & 0 & 0 & 0 & 0 & 1 \\ -\omega_{01}^2 & 0 & 0 & 0 & \dfrac{R_{g1}}{L_1} & 0 \\ 0 & -\omega_{02}^2 & 0 & -\dfrac{R_{g1}}{L_2} & 0 & \dfrac{R_{g2}}{L_2} \\ 0 & 0 & -\omega_{03}^2 & 0 & -\dfrac{R_{g2}}{L_3} & 0 \end{bmatrix}, \tag{15}$$

where $\underline{\mathbf{M}}$ is the six-by-six circuit matrix for the third-order circuit. Moreover, $\omega_{01} = 1/\sqrt{C_1 L_1}$, $\omega_{02} = 1/\sqrt{C_2 L_2}$, and $\omega_{03} = 1/\sqrt{C_3 L_3}$ are resonance angular frequencies of three isolated resonators (without coupling). The characteristic equation is expressed by

$$\begin{aligned} &\omega^6 - \omega^4 \left(\frac{R_{g2}^2}{L_2 L_3} - \frac{R_{g1}^2}{L_1 L_2} + \omega_{01}^2 + \omega_{02}^2 + \omega_{03}^2 \right) \\ &+ \omega^2 \left(\frac{R_{g2}^2 \omega_{01}^2}{L_2 L_3} - \frac{R_{g1}^2 \omega_{03}^2}{L_1 L_2} + \omega_{01}^2 \omega_{02}^2 + \omega_{01}^2 \omega_{03}^2 + \omega_{02}^2 \omega_{03}^2 \right) \\ &- \omega_{01}^2 \omega_{02}^2 \omega_{03}^2 = 0. \end{aligned} \tag{16}$$

For $R_{g1}=0$ and $R_{g2}=0$, the three series resonators are uncoupled, and the three circuits have three angular eigenfrequency pairs of $\omega_{1,4}=\pm\omega_{01}$, $\omega_{2,5}=\pm\omega_{02}$, and $\omega_{3,6}=\pm\omega_{03}$. As an example, we use the following component values to obtain third-order EPD: $L_1=1$ μH, $L_2=-33.33$ μH, $L_3=3.33$ mH, $C_1=3$ μF, $C_2=-30$ nF, $C_3=0.1$ nF, $R_{g1}=3.33$ Ω and $R_{g2}=333.33$ Ω. The obtained EPD frequency that corresponds to the mentioned component values is $\omega_e=10^6$ rad/s. The calculated results in Figures 2b and 2c show the real and imaginary parts of perturbed eigenfrequencies by solving the eigenvalue problem presented in equation (14). In these two plots, the first gyration resistance R_{g1} is perturbed near the EPD, and the calculated eigenfrequencies are normalized to the corresponding EPD frequency. Also, Figures 2d and 2e show analogous results by perturbing the second gyration resistance R_{g2}. Let's consider the first resonator to be a sensing resonator. We can quantify its perturbation due to variations of external parameters in the surrounding environment by measuring the changes in the eigenfrequencies. The calculated eigenfrequencies when perturbing either the capacitance or the inductance in the first resonator are displayed in Figures 2f and 2g and Figures 2h and 2i, respectively. The eigenfrequencies near the EPD are also estimated by using the Puiseux fractional power series expansion, as explained in Appendix D. According to the computed values in Figures 2b–2i, eigenfrequencies always have a negative imaginary part that shows instability. The green dashed lines in Figures 2b–2i represent the estimated results by the Puiseux series, which exhibit good agreement with the eigenvalues obtained directly from the eigenvalue problem in equation (14). The coefficient of the Puiseux series are calculated as, $\alpha_1=5.50\times10^5$ rad/s, and $\alpha_2=-5.05\times10^4$ rad/s when perturbing R_{g1}, $\alpha_1=2.75\times10^5+j4.77\times10^5$ rad/s, and $\alpha_2=-1.77\times10^5+j3.06\times10^5$ rad/s when perturbing R_{g2}, $\alpha_1=1.73\times10^5+j3.00\times10^5$ rad/s, and $\alpha_2=7.01\times10^4-j1.21\times10^5$ rad/s when perturbing C_1, and finally $\alpha_1=2.50\times10^5+j4.33\times10^5$ rad/s, and $\alpha_2=6.25\times10^4-j1.08\times10^5$ rad/s when perturbing L_1.

3 EPD in parallel configuration

This section analyzes various types of second-order EPD in the parallel configuration. First, we show the general condition for second-order EPD in the parallel configuration and complement the theoretical calculations using time-domain circuit simulators. Second, we show how to get an EPD with real frequency by coupling two unstable resonators, i.e., imaginary resonance frequencies. Next, we show how to obtain an EPD associated with instability, i.e., where the EPD frequency is purely imaginary. Finally, we get EPD in a circuit that two stable resonators coupled via asymmetric gyrator compared to the symmetric case.

3.1 Second-order EPD

In this configuration, two parallel LC tanks are coupled by an ideal gyrator, as displayed in Figure 3a. We first write the Kirchhoff current law equations describing current and voltages in terms of charges [58]

$$\begin{cases} \ddot{Q}_1 = -\dfrac{1}{C_1L_1}Q_1 + \dfrac{1}{R_gC_2}\dot{Q}_2 \\ \ddot{Q}_2 = -\dfrac{1}{C_2L_2}Q_2 - \dfrac{1}{R_gC_1}\dot{Q}_1 \end{cases}. \tag{17}$$

Introducing the state vector as $\Psi\equiv\left[Q_1,Q_2,\dot{Q}_1,\dot{Q}_2\right]^{\mathrm{T}}$ analogously to what was defined in the series configuration, leads to the following system of equations [58]

$$\frac{\mathrm{d}\Psi}{\mathrm{d}t}=\underline{\mathbf{M}}\Psi, \tag{18}$$

$$\underline{\mathbf{M}}=\begin{bmatrix} 0 & 0 & 1 & 0 \\ 0 & 0 & 0 & 1 \\ -\omega_{01}^2 & 0 & 0 & \dfrac{1}{R_gC_2} \\ 0 & -\omega_{02}^2 & -\dfrac{1}{R_gC_1} & 0 \end{bmatrix}. \tag{19}$$

The eigenfrequencies of the circuit are evaluated by solving the characteristic equation [58]

$$\omega^4-\omega^2\left(\omega_{01}^2+\omega_{02}^2+\frac{1}{C_1C_2R_g^2}\right)+\omega_{01}^2\omega_{02}^2=0. \tag{20}$$

All the coefficients are real, so ω and ω^* are both roots of the equation. Also, the characteristic equation is a quadratic equation in ω^2, so both ω and $-\omega$ are solutions. The angular eigenfrequencies are determined as [58]

$$\omega_{1,3}=\pm\sqrt{a+b},\ \omega_{2,4}=\pm\sqrt{a-b}, \tag{21}$$

$$a=\frac{1}{2}\left(\omega_{01}^2+\omega_{02}^2+\frac{1}{C_1C_2R_g^2}\right). \tag{22}$$

$$b^2=a^2-\omega_{01}^2\omega_{02}^2. \tag{23}$$

Based on equation (21), the EPD can be achieved when $b=0$ and the EPD angular frequency is $\omega_e=\sqrt{a}$. We assume $a>0$, so the EPD has a real angular frequency. Therefore, the condition to get EPD with real frequency is rewritten as [58]

$$\omega_{01}^2+\omega_{02}^2-\omega_{gp}^2>0, \tag{24}$$

where the equivalent gyrator frequency for the parallel circuit is defined as $\omega_{gp}^2=-1/\left(C_1C_2R_g^2\right)$. The following condition must be achieved to obtain EPD based on equations (21), (22), and (23), [58]

$$\left(\omega_{01}-\omega_{02}\right)^2=\omega_{gp}^2. \tag{25}$$

We investigate three cases to select the components' values. First, if ω_{01} and ω_{02} are purely real, so the value of either C_1 or C_2 should be negative to have the same sign on

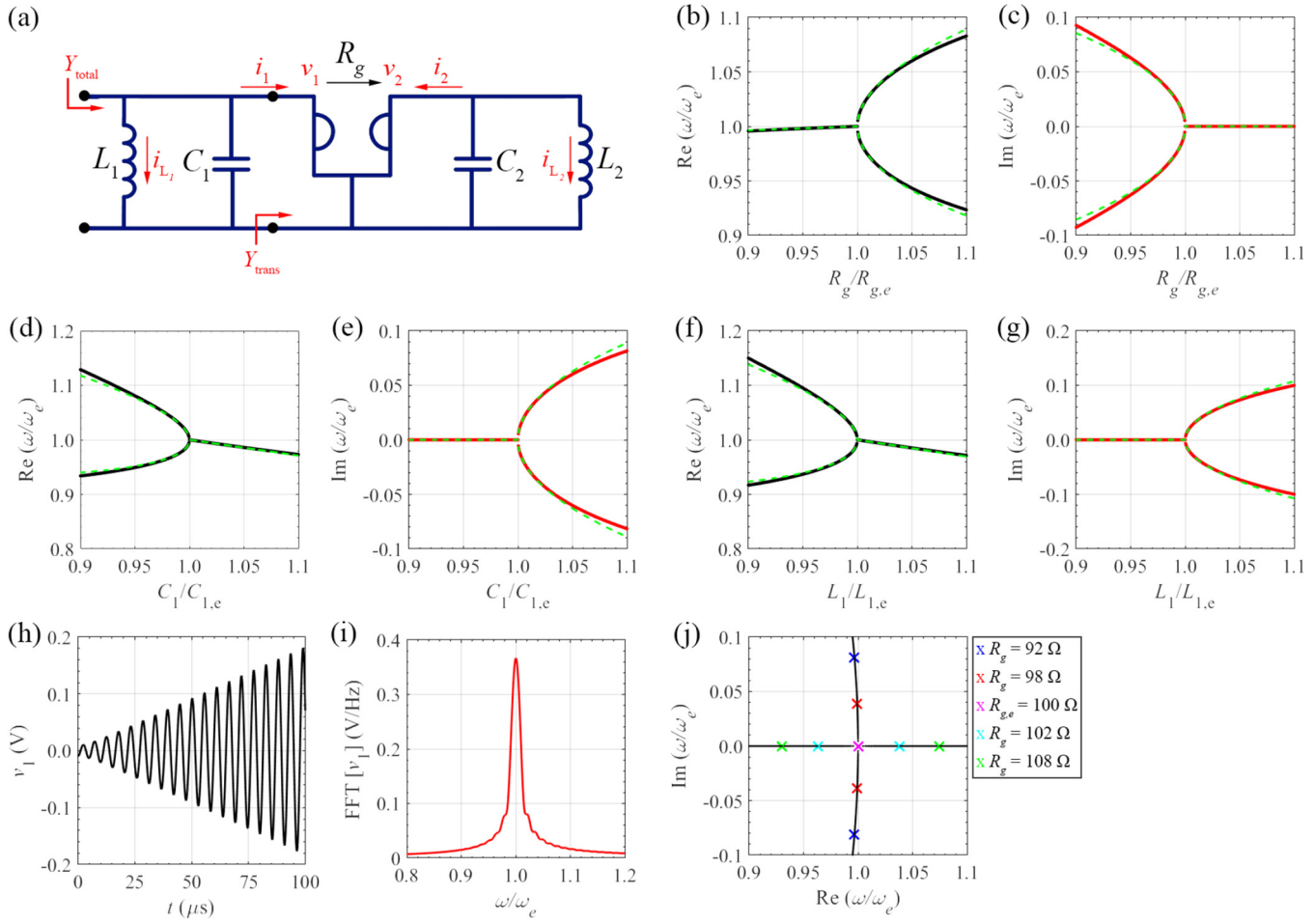

Fig. 3. (a) The schematic illustration of the gyrator-based circuit with the ideal gyrator in parallel configuration. In this circuit, two different LC resonators are used in a parallel configuration, coupled via an ideal gyrator. The sensitivity of the (b), (d), (f) real and (c), (e), (g) imaginary parts of the eigenfrequencies to (b), (c) gyration resistance, (d), (e) positive capacitance C_1 (f), (g) positive inductance L_1 perturbation. Solid lines: solution of eigenvalue problem of equation (18); green-dashed lines: Puiseux series approximation truncated to its second term. Voltage $v_1(t)$ under the EPD condition in the (h) time-domain, and (i) frequency-domain. The frequency-domain result is calculated by applying an FFT with 10^6 samples in the time window of 0 μs to 100 μs. (j) Root locus of zeros of $Y_{total}(\omega) = 0$ showing the real and imaginary parts of resonance frequencies of the circuit when perturbing gyration resistance. At the EPD, the system's total admittance is $Y_{total}(\omega) \propto (\omega - \omega_e)^2$; hence it shows a double zero at ω_e.

both sides of equation (25). As a result, to have a real value for ω_{01} and ω_{02}, one resonator needs to be composed of both negative C and L.

Second, if ω_{01} and ω_{02} have imaginary values, then C_1 and C_2 should have the same sign, either positive or negative. In this case, each resonator is unstable when uncoupled, and more details for this case are provided in Section 3.2.

Lastly, if only one of the ω_{01} or ω_{02} is imaginary, and the other is real; there is not any condition to obtain an EPD. In this section, we consider the first case in which one capacitor and one inductor on the same resonator have a negative value so ω_{gp}^2 is positive. When the EPD condition is satisfied, two eigenfrequencies coalesce at a real EPD angular frequency

$$\omega_e = \sqrt{\frac{1}{2}\left(\omega_{01}^2 + \omega_{02}^2 - \omega_{gp}^2\right)} = \sqrt{\omega_{01}\omega_{02}}. \qquad (26)$$

As an example, we use the following values for the components: $L_1 = 33\,\mu\text{H}$, $L_2 = -33\,\mu\text{H}$, $C_2 = -33\,\text{nF}$, and $R_g = 50\,\Omega$. The capacitance C_1 is determined by solving the quadratic equation from the EPD condition. There are two possible values of the capacitance C_1 that satisfies the EPD condition, and we select $C_1 = 15.43\,\text{nF}$ in this example. Then the corresponding value for EPD frequency is calculated as $\omega_e = 1.16 \times 10^6\,\text{rad/s}$. The calculated results in Figures 3b and 3c show the real and imaginary parts of the angular eigenfrequencies obtained from the eigenvalue problem when varying the gyrator resistance near the EPD. Moreover, the results in Figures 3d and 3e show the real and imaginary parts of eigenfrequencies when varying the positive capacitance C_1. Then, by varying the positive inductance L_1, the real and imaginary parts of eigenfrequencies are shown in Figures 3f and 3g. All the angular eigenfrequencies in the plots are normalized to the EPD

angular frequency. In addition, the eigenfrequencies are also estimated using the Puiseux fractional power series expansion to show the sensitivity of angular eigenfrequencies to perturbation. Appendix D provides additional details on this method. The calculated eigenfrequencies using the Puiseux fractional power series expansion are shown by the green dashed lines in Figures 3b–3g. The approximated results show excellent agreement compared to the solutions of the eigenvalue problem of equation (18). The coefficients of the Puiseux series up to second order are calculated as, $\alpha_1 = 3.13 \times 10^5$ rad/s, and $\alpha_2 = 4.24 \times 10^4$ rad/s when perturbing R_g, $\alpha_1 = j3.26 \times 10^5$ rad/s, and $\alpha_2 = -3.35 \times 10^5$ rad/s when perturbing C_1, $\alpha_1 = j3.94 \times 10^5$ rad/s, and $\alpha_2 = -3.57 \times 10^5$ rad/s when perturbing L_1. According to the obtained eigenfrequencies in Figures 3b and 3c, by varying R_g, the real part of the eigenfrequencies split when $R_g > R_{g,e}$ and the imaginary part of the eigenfrequencies splits when $R_g < R_{g,e}$. In addition, the results in Figures 3d–3g show that by perturbing C_1 and L_1, the dispersion diagram exhibits an analogous frequency behavior.

The time-domain simulation is provided using the Keysight ADS time-domain circuit simulator, and the voltage on the node v_1 is shown in Figure 3h. In the simulation, we use 1 mV as an initial voltage on the left capacitor C_1 and we use an ideal gyrator model. The voltage increases linearly with time, indicating that two circuit eigenfrequencies are coalescing, and the system signal is described by a double pole. The spectrum is calculated by using the FFT of the voltage $v_1(t)$ with 10^6 samples in the time window of 0 µs to 100 µs, and the result is shown in Figure 3i. According to Figure 3i, the oscillation frequency corresponds to $\omega_e = 1.16 \times 10^6$ rad/s, hence there is a very good agreement with the theoretical EPD angular frequency. In this example, the components are lossless.

We demonstrate how the EPD is related to the circuit's resonance, which can be recognized directly in a frequency-domain analysis. We calculate the circuit's total input admittance $Y_{total}(\omega)$ using the same method as we did for the series configuration. We define the admittances of the resonators as $Y_1 = j\omega C_1 + 1/(j\omega L_1)$, and $Y_2 = j\omega C_2 + 1/(j\omega L_2)$. Then the transferred admittance on the left side is calculated by (see Figure 3a)

$$Y_{trans}(\omega) = \frac{1}{R_g^2 Y_2}. \tag{27}$$

The total admittance observed from the circuit input port (see Figure 3a) is calculated by

$$Y_{total}(\omega) = Y_1(\omega) + Y_{trans}(\omega). \tag{28}$$

The resonant angular frequencies are obtained by solving $Y_{total}(\omega) = 0$. The resonance frequencies by perturbing gyration resistance values are calculated in Figure 3j, normalized to the EPD angular frequency. Considering the gyrator resistance value at the EPD, two zeros coincide, representing the point where the two curves meet exactly at the EPD angular frequency. According to Figure 3j, for $R_g < R_{g,e}$, the resonance angular frequencies are complex conjugate pairs, and for $R_g > R_{g,e}$, the resonance angular frequencies are purely real.

3.2 Stable EPD frequency via unstable uncoupled resonators

This section employs unstable resonators to obtain an EPD with real eigenfrequency. In other words, we study the case of two unstable resonators coupled via an ideal gyrator. This issue can be investigated in both series and parallel configurations; here, we look at the case with the parallel configuration. A comprehensive analysis of the unstable resonators for series configuration is presented in [57]. The analysis in this section is analogous to one in Section 3.1. Each resonator should have only one component with a negative value to have an unstable resonance frequency. Without loss of generality, we consider a negative value for both inductances and a positive value for both capacitances; hence, ω_{gs}^2 has negative value. Based on the condition for EPD ($b = 0$) and by using equation (23), the first and second terms in equation (22) are negative, and the third term is positive. According to equation (26), if $|\omega_{01}^2 + \omega_{02}^2| < \omega_{gp}^2$ the calculated EPD frequency will be real, and if $|\omega_{01}^2 + \omega_{02}^2| > \omega_{gp}^2$, the EPD frequency yields an imaginary value.

In order to obtain EPD with real frequency by using unstable resonators, we use the following set of values for components: $L_1 = -33$ µH, $L_2 = -33$ µH, $C_1 = 2.32$ nF, $C_2 = 33$ nF, and $R_g = 25\ \Omega$. Therefore, both ω_{01}^2 and ω_{02}^2 have negative values, with $\omega_{01} = -j3.62 \times 10^6$ rad/s, and $\omega_{02} = -j9.58 \times 10^5$ rad/s. The used value for components leads to a real EPD angular frequency of $\omega_e = 1.86 \times 10^6$ rad/s. The normalized eigenfrequencies by solving the eigenvalue problem of equation (18) while perturbing R_g, C_1, and L_1 are shown in Figures 4a–4f. In addition, the eigenfrequencies are estimated using the Puiseux fractional power series expansion to confirm the calculated results. More information for the Puiseux series is provided in Appendix D. The calculated eigenfrequencies using the Puiseux series are drawn by the green dashed lines in Figures 4a–4f. To calculate the estimated eigenfrequencies, the coefficients of the Puiseux series are calculated as, $\alpha_1 = j3.24 \times 10^6$ rad/s, and $\alpha_2 = -2.81 \times 10^6$ rad/s when perturbing R_g, $\alpha_1 = j1.05 \times 10^6$ rad/s, and $\alpha_2 = -7.60 \times 10^5$ rad/s when perturbing C_1, $\alpha_1 = 2.03 \times 10^6$ rad/s, and $\alpha_2 = 6.46 \times 10^5$ rad/s when perturbing L_1. The calculated results in Figures 4a–4d demonstrate that by perturbing R_g and C_1, the circuit shows the analogous frequency behavior. So, when the component value is smaller than the EPD value, the real parts of the eigenfrequencies split, and when the component value is bigger than the EPD value, the imaginary parts of the eigenfrequencies split. According to the obtained eigenfrequencies in Figures 4e and 4f, by varying L_1, the real part of the eigenfrequencies split when $L_1 > L_{1,e}$ and the imaginary part of the eigenfrequencies split when $L_1 < L_{1,e}$.

We use the Keysight ADS circuit simulator to analyze the time-domain response of the circuit under EPD conditions. The transient response of the coupled resonators with the ideal gyrator is simulated using the time-domain solver with an initial condition $v_1(0) = 1$ mV, where $v_1(t)$ is the voltage of the capacitor in the left resonator (see Figure 3a). Figure 4g shows the time-domain simulation results of the voltage $v_1(t)$. The voltage is obtained in the period of 0 ms to 100 µs. As previously

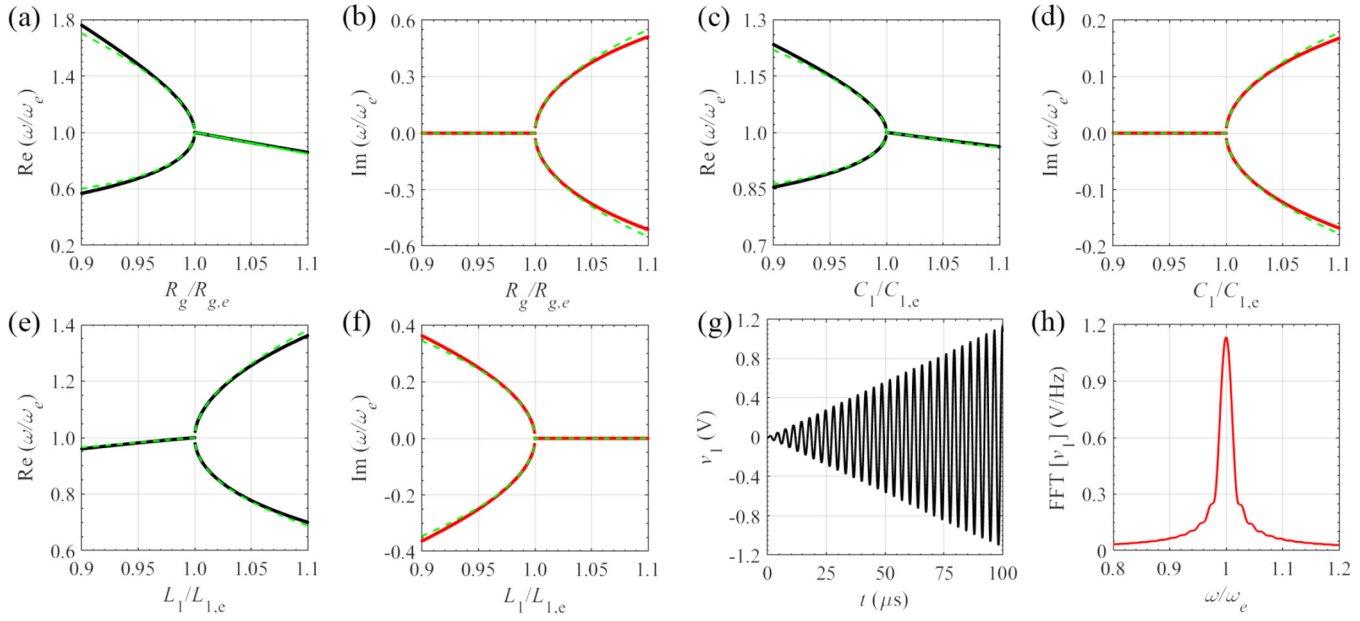

Fig. 4. The sensitivity of the (a), (c), (e) real and (b), (d), (f) imaginary parts of the eigenfrequencies to (a), (b) gyration resistance, (c), (d) positive capacitance C_1 (e), (f) positive inductance L_1 perturbation. Solid lines: solution of eigenvalue problem of equatoin (18); green-dashed lines: Puiseux series approximation truncated to its second term. Here, both resonators are unstable, i.e., resonance frequency of resonators is purely imaginary. Voltage $v_1(t)$ under the EPD condition in the (g) time-domain, and (h) frequency-domain. The frequency-domain result is calculated by applying an FFT with 10^6 samples in the time window of 0 μs to 100 μs.

stated, the solution of the eigenvalue problem at the EPD differs from any other regular frequency in the dispersion diagram because the circuit matrix contains repeated eigenvalues associated with one eigenvector. As a result, the voltage increases linearly with increasing time, while the oscillation frequency remains constant. It is the consequence of coalescing eigenvalues and eigenvectors, which correspond to a double pole or a zero in the circuit, depending on the observed parameter. The spectrum is calculated by using the FFT of the voltage $v_1(t)$ with 10^6 samples in the time window of 0 μs to 100 μs, and the calculated result is shown in Figure 4h. According to Figure 4h, the oscillation frequency corresponds to $\omega_e = 1.86 \times 10^6$ rad/s, so there is a very good agreement with the theoretical EPD angular frequency. In the presented example, all components were ideal, and we did not consider any lossy element in the circuit. A comprehensive study for the effect of losses in the stability of the circuit with unstable resonators is presented in [57].

3.3 Unstable EPD frequency

So far, we have focused on the EPD with real frequency, which is a practical case due to the stability of the resonance frequency. This section analyzes the case with unstable EPD frequency, i.e., EPD with imaginary frequency. Here we investigate the example for second-order EPD in the parallel configuration. The required analysis in this section is the same as the discussion presented in Section 3.1. The only difference is that the selected value for components leads to imaginary EPD frequency.

As an example, we use the following values for the components: $L_1 = 15\,\mu\text{H}$, $L_2 = -50\,\mu\text{H}$, $C_2 = -15\,\text{nF}$, and $R_g = 25\,\Omega$. The capacitance C_1 is obtained by solving the quadratic equation from the EPD condition. There are two possible values for C_1 that satisfies the EPD condition, and we select $C_1 = 3.50\,\text{nF}$ in this example. Then the corresponding value for EPD frequency is calculated as $\omega_e = j2.24 \times 10^6\,\text{rad/s}$, which shows that the circuit is unstable at EPD. The results in Figures 5a and 5b show the real and imaginary parts of perturbed eigenfrequencies calculated from the eigenvalue problem when varying the gyration resistance near the EPD. Also, the obtained results in Figures 5c and 5d show the real and imaginary parts of eigenfrequencies by perturbing the positive capacitance C_1. Then, by perturbing the positive inductance L_1, the real and imaginary parts of eigenfrequencies are shown in Figures 5e and 5f. The calculated eigenfrequencies in these plots are normalized to the absolute value of imaginary EPD frequency. In addition, the eigenfrequencies are calculated using the Puiseux fractional power series expansion. Appendix D contains further information on this method. The obtained eigenfrequencies using the Puiseux series are shown by the green dashed lines in Figures 5a–5f. The estimated results show perfect agreement compared to the solutions of the eigenvalue problem in equation (18). In the calculated estimated eigenfrequencies, the coefficients of the Puiseux series are

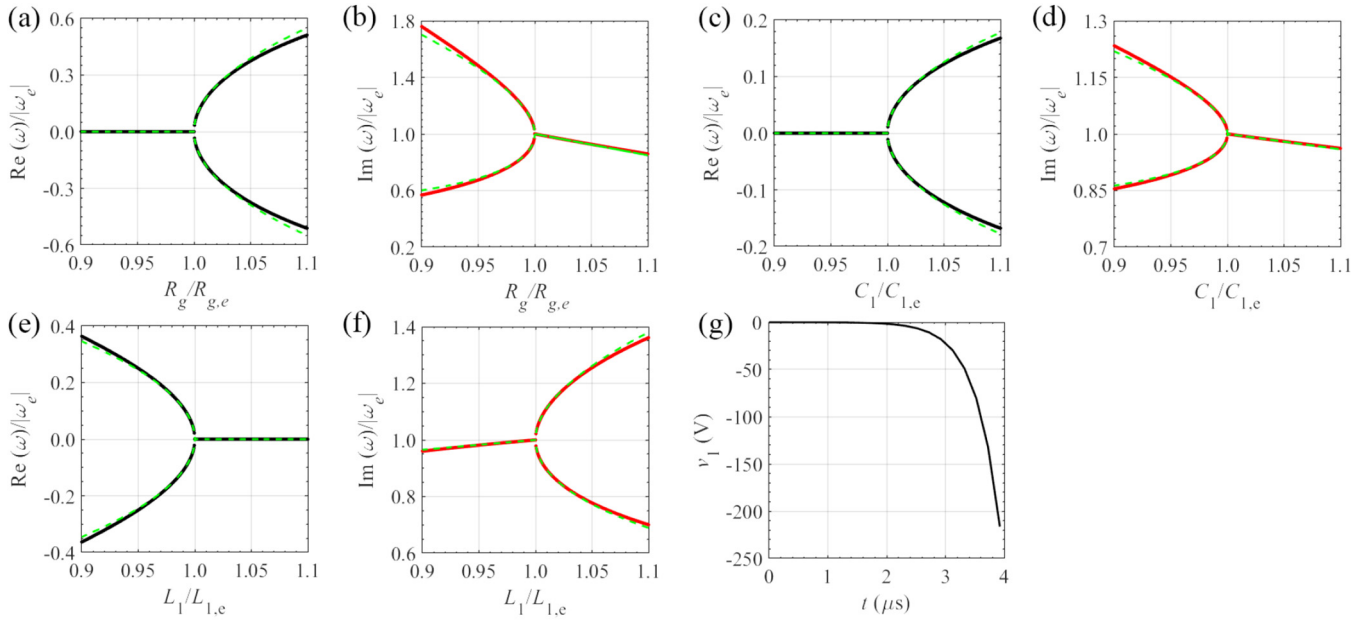

Fig. 5. The sensitivity of the (a), (c), (e) real and (b), (d), (f) imaginary parts of the eigenfrequencies to (a), (b) gyration resistance, (c), (d) positive capacitance C_1 (e), (f) positive inductance L_1 perturbation. Solid lines: solution of eigenvalue problem of equation (18); green-dashed lines: Puiseux series approximation truncated to its second term. Here, the EPD frequency is unstable, i.e., EPD frequency is purely imaginary. (g) Voltage $v_1(t)$ for the unstable EPD condition in the time-domain, which increases exponentially over time.

calculated as, $\alpha_1 = 3.90 \times 10^6$ rad/s, and $\alpha_2 = -j3.39 \times 10^6$ rad/s when perturbing R_g, $\alpha_1 = 1.26 \times 10^6$ rad/s, and $\alpha_2 = -j9.16 \times 10^5$ rad/s when perturbing C_1, $\alpha_1 = j2.45 \times 10^6$ rad/s, and $\alpha_2 = j7.78 \times 10^5$ rad/s when perturbing L_1. Using the ideal model for the gyrator, the time-domain simulation result for the node voltage v_1 in Figure 5g is obtained using the Keysight ADS circuit simulator. We use 1 mV as an initial voltage on the capacitor C_1. The voltage exponentially increases over time without any oscillation, indicating that the circuit is unstable.

3.4 Asymmetric Gyrator

In this section, two parallel LC tanks are coupled by an asymmetric gyrator with the forward gyration resistance of R_{gf} and backward gyration resistance of R_{gb}, as displayed in Figure 6a. The concept of asymmetry in the gyrator is discussed in Appendix E. We find the EPD condition by writing the Kirchhoff current law equations and finding the Liouvillian matrix. As a result, the following equations are written by describing currents and voltages in terms of charges

$$\begin{cases} \ddot{Q}_1 = -\dfrac{1}{C_1 L_1} Q_1 + \dfrac{1}{R_{gb} C_2} \dot{Q}_2 \\ \ddot{Q}_2 = -\dfrac{1}{C_2 L_2} Q_2 - \dfrac{1}{R_{gf} C_1} \dot{Q}_1 \end{cases}. \tag{29}$$

By defining the state vector as $\Psi \equiv \left[Q_1, Q_2, \dot{Q}_1, \dot{Q}_2\right]^{\mathrm{T}}$, we represent equations in Liouvillian form

$$\frac{\mathrm{d}\Psi}{\mathrm{d}t} = \underline{\mathbf{M}}\Psi, \tag{30}$$

$$\underline{\mathbf{M}} = \begin{bmatrix} 0 & 0 & 1 & 0 \\ 0 & 0 & 0 & 1 \\ -\omega_{01}^2 & 0 & 0 & \dfrac{1}{R_{gb} C_2} \\ 0 & -\omega_{02}^2 & -\dfrac{1}{R_{gf} C_1} & 0 \end{bmatrix}. \tag{31}$$

The eigenfrequencies of the circuit are calculated by solving the below characteristic equation

$$\omega^4 - \omega^2 \left(\omega_{01}^2 + \omega_{02}^2 + \frac{1}{R_{gb} R_{gf} C_1 C_2} \right) + \omega_{01}^2 \omega_{02}^2 = 0. \tag{32}$$

Then the angular eigenfrequencies are determined as

$$\omega_{1,3} = \pm\sqrt{a+b}, \omega_{2,4} = \pm\sqrt{a-b}, \tag{33}$$

$$a = \frac{1}{2}\left(\omega_{01}^2 + \omega_{02}^2 + \frac{1}{C_1 C_2 R_{gb} R_{gf}} \right). \tag{34}$$

$$b^2 = a^2 - \omega_{01}^2 \omega_{02}^2. \tag{35}$$

According to equation (33), the EPD is achieved when $b = 0$. The following condition must be met to achieve EPD in the asymmetric configuration using equations (34), and (35)

$$(\omega_{01} - \omega_{02})^2 = -\frac{1}{C_1 C_2 R_{gb} R_{gf}}. \tag{36}$$

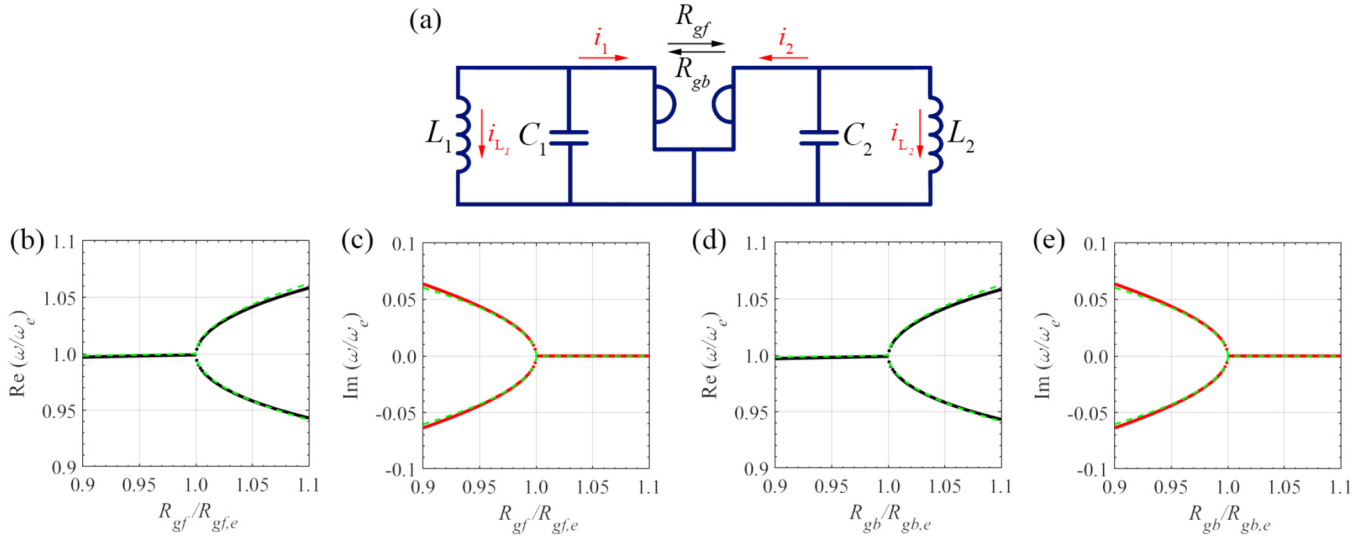

Fig. 6. (a) The schematic illustration of the gyrator-based circuit with the assymetric gyrator in parallel configuration. The sensitivity of the (b), (d), real and (c), (e), imaginary parts of the eigenfrequencies to (b), (c) forward gyration resistance and (d), (e) backward gyration resistance. Solid lines: solution of eigenvalue problem of equation (30); green-dashed lines: Puiseux series approximation truncated to its second term.

When the EPD condition is satisfied, two eigenfrequencies coalesce at a real EPD angular frequency

$$\omega_e = \sqrt{\frac{1}{2}\left(\omega_{01}^2 + \omega_{02}^2 + \frac{1}{C_1 C_2 R_{gb} R_{gf}}\right)} = \sqrt{\omega_{01}\omega_{02}}. \quad (37)$$

Here we use the values derived for parallel configuration in Section 3.1 where $L_1 = 33\,\mu\text{H}$, $L_2 = -33\,\mu\text{H}$, $C_1 = 15.43\,\text{nF}$, $C_2 = -33\,\text{nF}$, $R_{gf} = 100\,\Omega$, and $R_{gb} = 100\,\Omega$. Then the EPD frequency is calculated as $\omega_e = 1.16 \times 10^6 \text{rad/s}$. The results in Figures 6b and 6c show the real and imaginary parts of perturbed eigenfrequencies obtained from the eigenvalue problem of equation (30) when varying the forward gyrator resistance near the EPD value and Figures 6d and 6e are eigenfrequency evolution by varying the backward gyration resistance. All the obtained eigenfrequencies in the mentioned plots are normalized to the EPD frequency. In addition, the eigenfrequencies are calculated using the Puiseux fractional power series expansion to measure the sensitivity of the eigenfrequencies to perturbation, and the calculated eigenfrequencies are drawn by the green dashed lines. Appendix D provides additional information on this method. In the presented estimated result, the coefficients of the Puiseux series are calculated as, $\alpha_1 = 2.21 \times 10^5\,\text{rad/s}$, and $\alpha_2 = 2.12 \times 10^4\,\text{rad/s}$ when perturbing R_{gb} or R_{gf}. As we demonstrate for symmetric case in Section 3.1, by varying R_g, the real part of the eigenfrequencies split when $R_g > R_{g,e}$, and the imaginary part of the eigenfrequencies split when $R_g < R_{g,e}$. In addition, the calculated eigenfrequencies in Figures 6b–6e demonstrate that by perturbing R_{gf} and R_{gb}, the gyrator-based circuit shows the analogous frequency behavior. On the other hand, we know that higher sensitivity is achieved when the bifurcation of the dispersion diagrams is wider [60]. So, by comparing the symmetric and asymmetric cases, it is clear that the symmetric case is more sensitive than the asymmetric case.

4 Conclusion

We have provided a comprehensive description of a new technique based on using gyrators and resonators to get EPDs. This new method opens up a new way to realize EPDs offering many new circuit configurations complementary to those satisfying PT symmetry.

We have shown various circuits based on resonators coupled via gyrators that support an EPD, where some resonators are made of negative inductance and negative capacitance that can be realized using operational amplifiers. We have provided the theoretical conditions for second-order EPD to exist with either purely real or imaginary frequency. We have complemented our theoretical calculations with time-domain circuit simulations, showing an excellent agreement. We have shown how to obtain a stable second-order EPD by using two unstable (when isolated) coupled resonators and also using two stable resonators coupled via an asymmetric gyrator. We have demonstrated that the eigenfrequencies are extremely sensitive to the circuit's perturbation, which may have important implications for ultrasensitive sensing technologies and RF sensors. An important feature is that when we perturb a circuit component (e.g., a capacitor), the circuit provides two shifted frequencies with real values, contrary to the case of EPD based on PT symmetry where the two shifted frequencies are complex valued.

In this paper, the lossless circuits are analyzed, whereas the effects of additional loss or gain on each resonator for some configurations have been investigated in [57,58]. Any

loss or gain in the circuit leads to complex-valued eigenfrequencies, which cause instability and start an oscillatory regime. To prevent the circuit from saturating and still using the high sensitivity advantage, we could switch on and off the circuit and work in the transient regime as was done in [27].

Higher sensitivity is achieved using third-order EPD, with the important property that the circuit is always unstable, which is a feature that can be exploited to make an oscillator based on an EPD. Based on duality theory, all the cases mentioned above can be explored for both series and parallel resonators. Calculating the relevant Puiseux fractional power series expansion for all the cases shows the EPD's occurrence and the circuit's sensitivity when operating at the EPD. We believe that the demonstrated results pave the way for conceivable new operation strategies for boosting the overall performance of high-sensitive sensors.

This material is based upon work supported by the National Science Foundation (NSF) under Grant No. ECCS-1711975 and by the Air Force Office of Scientific Research (AFOSR) Grant No. FA9550-19-1-0103.

Appendix A: Gyrator implementation

A gyrator is a nonreciprocal component, so any gyrator network should include at least one nonreciprocal component [61]. The gyrator network can be realized using a medium consisting of particles carrying permanent electric and permanent magnetic dipoles or through a gyromagnetic effect of a ferromagnetic medium [37]. There is an apparent need to develop a gyrator circuit that is antireciprocal with extremely low input and output impedances [37]. Various methods of realization are suggested for the gyrator, such as the Hall-effect gyrator, but the most practical are those based on transistors or other electronic active devices designed to operate as amplifiers.

Nowadays, the well-known nonreciprocal component is a transistor or a combination of transistors as integrated opamps. These components are found in almost all suitable gyrator circuits [61]. Also, it is not possible to implement an efficient gyrator with only one amplifier [61]. Many published transistor-based gyrator circuits can be integrated [38–45], but because a special-purpose integrated circuit must be manufactured, the cost per device is expected to be significant. However, integrated-circuit opamps are commonly available as off-the-shelf components, and they are inexpensive, so they can be used to design practical gyrators [46–53]. As a result, they may be used to make low-cost hybrid gyrator circuits.

The ideal gyrator's admittance matrix may be divided up to realize a gyrator as [42,44]

$$\begin{bmatrix} 0 & G_g \\ -G_g & 0 \end{bmatrix} = \begin{bmatrix} 0 & G_g \\ 0 & 0 \end{bmatrix} + \begin{bmatrix} 0 & 0 \\ -G_g & 0 \end{bmatrix}. \tag{A1}$$

Voltage-controlled current sources can be used to make the two independent off-diagonal transconductances. This can be achieved by connecting two amplifiers to make a closed loop. In this circuit, the first amplifier has a phase change from input to the output of zero, while the second has π. Moreover, the input and output impedances of each amplifier are both high. The main diagonal terms on the gyrator matrix are kept to small magnitudes by high impedances [42]. In [42], a gyrator in an integration-ready form has been built. The proposed gyrator could make inductances with Q-factors of 500 produced by capacitors, and the circuit is highly stable. By providing an active feedback path, Shenoi has developed a gyrator circuit with only three transistors [45]. The circuit operates as a two-way feedback system with transfer admittance parameters equal in magnitude and opposite in phase [45]. Sheahan et al. also created a high-quality gyrator that can operate at frequencies up to 100 kHz [38]. This circuit allows temperature-independent and high Q-factor inductance generation from a low-loss, integratable capacitor [38]. In [44], the design of a new integratable high-performance direct-coupled gyrator circuit is explained, as well as other design features. Simulated inductances of up to 200 H are reached in the proposed design, with stable Q-factors of several thousand. Yanagisawa et al. propose a straightforward way for constructing an active gyrator based on two controlled-current sources [39]. A simplified experiment features inherent negative input and output resistances in this work, leading to optimal impedance-inverting properties. Moreover, in [40], an integrated gyrator circuit uses one diode, 12 resistors, and nine transistors (two of them are lateral PNP). The gyration resistance, input impedance, and resonant-circuit Q-factor obtained from experimental data show outstanding agreement with theory [40].

Because of the current state of technology, opamp-based gyrators are the most feasible design method for gyrators. For instance, Antoniou designed an ideal negative-impedance invertor using a voltage-controlled voltage source [46]. A practical circuit based on an opamp is used to demonstrate the suggested technique. To develop new gyrator circuits, it is used with negative-impedance convenors [46]. In [50], negative-impedance convertors and negative-impedance invertors are used to make equivalent circuits for gyrators. This paper presents a stability analysis of gyrator circuits, as well as a proof of a relevant passivity theorem [50].

Finally, one of the most practical and straightforward circuits to realize an ideal gyrator using opamp is proposed in [53]. A capacitively terminated opamp-based gyrator circuit model is derived using a typical range of amplifier specifications. Also, amplifier imperfections such as finite input and output resistances, as well as finite frequency-dependent amplification, are also taken into account in this model [53]. Experimentation and an exact computer-based analysis are used to confirm the model's validity. The model demonstrates how each amplifier imperfection affects the gyrator circuit's performance. By using ideal amplifiers, the Y-parameters of the gyrator circuit are

obtained as [53]

$$\underline{\mathbf{Y}} = \begin{bmatrix} 0 & \frac{R_4}{R_1 R_2} \\ -\frac{1}{R_3} & 0 \end{bmatrix}, \tag{A2}$$

which R_n ($n = 1, \ldots, 4$) are the resistors used in the proposed circuit [53]. All that is required to fabricate the circuit is a thin-film or thick-film substrate with four resistors and a chip dual. The amplifier and substrate are affordable, resulting in a low-cost gyrator circuit. Furthermore, the presented results in [53] show that only one of the four resistors can be trimmed to change the gyration resistance.

The gyrator can also be realized at higher frequencies. The nonreciprocal property of the Faraday effect is indeed used to realize a microwave circuit element analogous to Tellegen's gyrator [62,63], using a combination of ferrite material and twisted waveguide. Gyrators could be realized by also using magnetless nonreciprocal metamaterial [64,65].

Appendix B: Gyrator

A gyrator is a two-port component defined by its gyration resistance value that connects an input port to an output port. This two-port network converts circuits at the gyrator output into their dual regarding the gyration resistance value [53,66,67]. This component can cause a capacitive circuit to behave inductively and a parallel LC resonator to act like a series LC resonator. Gyrator enables the development of two-port devices that would otherwise be impossible to build with only the basic components, i.e., resistors, capacitors, inductors, and transformers. The gyrator, unlike the other four conventional elements, is nonreciprocal. Moreover, the gyrator could be considered a more fundamental circuit component than the ideal transformer because an ideal transformer can be made by cascading two ideal gyrators, but transformers cannot make a gyrator. The circuit symbol for this component is illustrated in Figure B1a. The voltage on one port is linked to the current on the other in an ideal gyrator and vice versa. So, the voltages and currents are converted by [45]

$$\begin{cases} v_2(t) = R_g i_1(t) \\ v_1(t) = -R_g i_2(t) \end{cases}. \tag{B1}$$

The gyration resistance R_g is the crucial parameter of the gyrator, which has a unit of ohm, and it has a gyration direction shown by an arrow in the circuit symbol. Although a gyrator is defined by its gyration resistance value, an ideal gyrator is a lossless element. A gyrator is a nonreciprocal component that can be determined by an antisymmetric impedance matrix as

$$\underline{\mathbf{Z}}_g = \begin{bmatrix} 0 & -R_g \\ R_g & 0 \end{bmatrix}. \tag{B2}$$

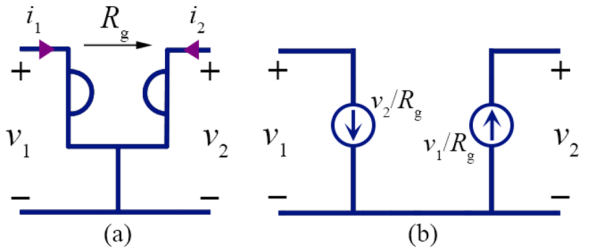

Fig. B1. (a) Gyrator schematic circuit symbol and corresponding voltages, currents, and gyration resistance direction. (b) Equivalent circuit for an ideal gyrator by using two dependent current sources.

Also, we can characterize it by admittance matrix as

$$\underline{\mathbf{Y}}_g = \begin{bmatrix} 0 & G_g \\ -G_g & 0 \end{bmatrix}, \tag{B3}$$

where $G_g = 1/R_g$ is gyration conductance. The aforementioned equations show that the gyration impedance and direction may be determined by connecting a voltage source to one port and measuring the current through a short circuit to another [68]. Therefore, we can model the gyrator using two dependent current sources, as shown in Figure B1b.

Appendix C: Impedance inverter implementation

Many circuits can generate the negative capacitances and inductances required by gyrator-based EPD circuits. Simple opamp-based circuits can be used as impedance inverters. Here, we show two well-known circuits that can be used to achieve negative capacitance and inductance. The circuit in Figure C1a converts the impedance $Z(\omega)$ to $Z_{in}(\omega) = -Z(\omega)$. When $Z(\omega)$ in Figure C1a is a single capacitor, i.e., $Z(\omega) = 1/(j\omega C)$, we obtain $Z_{in}(\omega) = -1/(j\omega C)$ at the input port. Moreover, we realize a negative inductance using a single capacitor. In this case, the circuit displayed in Figure C1b is utilized, leading to $Z_{in}(\omega) = -(R^2 C)\, j\omega$. This scheme obtains the desired negative inductance value by selecting proper values for resistances and capacitance.

Appendix D: Puiseux fractional power series expansion

The sensitivity of a system to a specific parameter may be detectable where the perturbation on the system changes observable quantities such as the system's resonance frequency. Changes in the system will be detected by measuring frequency changes and determining their relationship to perturbation. Puiseux fractional power series expansion helps us to find this relation for eigenvalues in the vicinity of EPD. For EPDs, sensitivity is boosted because of

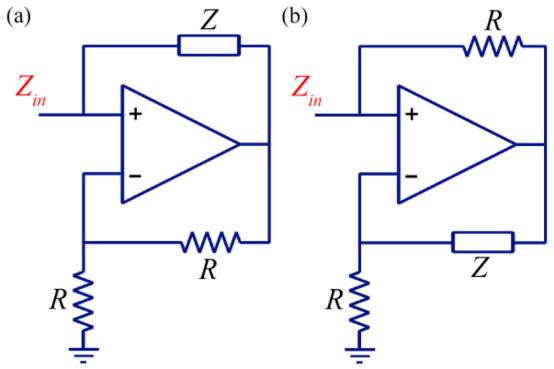

Fig. C1. Impedance inverter circuit by using an opamp to obtain (a) a negative capacitance, and (b) a negative inductance by using single capacitor as a load.

the eigenvalue's degeneracy. We consider a small perturbation Δ_X of a system parameter X as

$$\Delta_X = \frac{X - X_e}{X_e}, \tag{D1}$$

where X_e is the parameters's value at EPD, and X is the parameter's value after applying perturbation. A perturbation Δ_X to a system parameter results in a perturbed system matrix $\underline{\mathbf{M}}(\Delta_X)$, which results in perturbed eigenfrequencies $\omega_p(\Delta_X)$ with $p = 1, \ldots, n$ close to the n-th order EPD angular frequency. The perturbed eigenfrequencies near an EPD are found using a Puiseux fractional power series expansion [4]. A Puiseux series is a generalized power series with fractional and negative exponents in one variable. The Puiseux fractional power series expansion of $\omega_p(\Delta_X)$ is defined by [69]

$$\omega_p(\Delta_X) \approx \omega_e + \sum_{k=1}^{\infty} \alpha_k \left(\left(e^{j\frac{2\pi}{n}} \right)^p \Delta_X^{\frac{1}{n}} \right)^k, \tag{D2}$$

where the first two coefficients for the second-order approximation are expressed as [69]

$$\alpha_1 = \left(- \frac{\frac{\partial H(\Delta_X,\omega)}{\partial \Delta_X}}{\frac{1}{n!}\frac{\partial^n H(\Delta_X,\omega)}{\partial \omega^n}} \right)^{\frac{1}{n}}, \tag{D3}$$

$$\alpha_2 = - \frac{\alpha_1^{n+1} \frac{1}{(n+1)!} \frac{\partial^{n+1} H(\Delta_X,\omega)}{\partial \omega^{n+1}} + \alpha_1 \frac{\partial^2 H(\Delta_X,\omega)}{\partial \omega \partial \Delta_X}}{n\alpha_1^{n-1} \left(\frac{1}{n!} \frac{\partial^n H(\Delta_X,\omega)}{\partial \omega^n} \right)}. \tag{D4}$$

The coefficients are calculated at the EPD, where $\Delta_X = 0$, $\omega = \omega_e$, and $H(\Delta_X, \omega) = \det(\underline{\mathbf{M}}(\Delta_X) - j\omega \underline{\mathbf{I}})$.

In this paper, we utilize this series expansion for the second-order and third-order EPD. For second-order EPD, we express Puiseux fractional power series expansion by

$$\omega_p(\Delta_X) \approx \omega_e + \alpha_1 (-1)^p \sqrt{\Delta_X} + \alpha_2 \Delta_X, \tag{D5}$$

$$\alpha_1 = \sqrt{-2 \frac{\frac{\partial H(\Delta_X,\omega)}{\partial \Delta_X}}{\frac{\partial^2 H(\Delta_X,\omega)}{\partial \omega^2}}}, \tag{D6}$$

$$\alpha_2 = - \frac{\alpha_1^2 \frac{1}{6} \frac{\partial^3 H(\Delta_X,\omega)}{\partial \omega^3} + \frac{\partial^2 H(\Delta_X,\omega)}{\partial \omega \partial \Delta_X}}{\frac{\partial^2 H(\Delta_X,\omega)}{\partial \omega^2}}. \tag{D7}$$

Moreover, for third-order EPD, we calculate Puiseux fractional power series expansion by

$$\omega_p(\Delta_X) \approx \omega_e + \alpha_1 \left(e^{j\frac{2\pi}{3}} \right)^p \sqrt[3]{\Delta_X} + \alpha_2 \left(e^{j\frac{4\pi}{3}} \right)^p \sqrt[3]{(\Delta_X)^2}, \tag{D8}$$

$$\alpha_1 = \sqrt[3]{-6 \frac{\frac{\partial H(\Delta_X,\omega)}{\partial \Delta_X}}{\frac{\partial^3 H(\Delta_X,\omega)}{\partial \omega^3}}}, \tag{D9}$$

$$\alpha_2 = - \frac{\alpha_1^3 \frac{1}{24} \frac{\partial^4 H(\Delta_X,\omega)}{\partial \omega^4} + \frac{\partial^2 H(\Delta_X,\omega)}{\partial \omega \partial \Delta_X}}{\alpha_1 \left(\frac{1}{2} \frac{\partial^3 H(\Delta_X,\omega)}{\partial \omega^3} \right)}. \tag{D10}$$

Appendix E: Asymmetric gyrator

Although the gyrator is described by its gyration resistance value with the unit of ohm, it is a lossless component. The instantaneous power of the gyrator is calculated as

$$p(t) = v_1 i_1 + v_2 i_2 = (-R_g i_2) i_1 + (R_g i_1) i_2 = 0. \tag{E1}$$

The gyrator can be generalized to an asymmetric form, in which the forward and backward gyration resistances are different. The asymmetric gyrator impedance matrix is defined as

$$\underline{\mathbf{Z}} = \begin{bmatrix} 0 & -R_{gf} \\ R_{gb} & 0 \end{bmatrix}, \tag{E2}$$

where R_{gf} is forward gyration resistance and R_{gb} is backward gyration resistance. Devices for the condition that R_{gf} does not equal R_{gb} are referred to as *active gyrators*. Indeed, this is no longer a passive circuit component since the net instantaneous power is different

from zero,

$$p(t) = v_1 i_1 + v_2 i_2 = \left(-R_{gf} i_2\right) i_1 + \left(R_{gb} i_1\right) i_2 = i_1 i_2 \left(R_{gb} - R_{gf}\right) \neq 0. \tag{E3}$$

This asymmetric network can be realized by the circuit proposed in [53]. In order to realize asymmetric gyrator, we should consider proper value for resistors, so we have [53]

$$\begin{cases} R_{gf} = R_3 \\ R_{gb} = \dfrac{R_1 R_2}{R_4} \end{cases} \tag{E4}$$

where R_n $(n = 1, \ldots, 4)$ are the resistors used in the proposed circuit for the gyrator [53].

References

1. M.I. Vishik, L.A. Lyusternik, The solution of some perturbation problems for matrices and selfadjoint or non-selfadjoint differential equations I, Russ. Math. Surv. **15**, 1 (1960)
2. P. Lancaster, On eigenvalues of matrices dependent on a parameter, Numer. Math. **6**, 377 (1964)
3. A.P. Seyranian, Sensitivity analysis of multiple eigenvalues, J. Struct. Mech. **21**, 261 (1993)
4. T. Kato, *Perturbation Theory for Linear Operators* (Springer-Verlag, New York Inc., 1966)
5. W.D. Heiss, The physics of exceptional points, J. Phys. A **45**, 444016 (2012)
6. W.D. Heiss, Exceptional points of non-Hermitian operators, J. Phys. A **37**, 2455 (2004)
7. W.D. Heiss, Exceptional points – their universal occurrence and their physical significance, Czechoslovak J. Phys. **54**, 1091 (2004)
8. W.D. Heiss, Green's functions at exceptional points, Int. J. Theor. Phys. **54**, 3954 (2015)
9. J. Schnabel, H. Cartarius, J. Main, G. Wunner, W.D. Heiss, PT-symmetric waveguide system with evidence of a third-order exceptional point, Phys. Rev. A **95**, 053868 (2017)
10. J. Wiersig, Sensors operating at exceptional points: general theory, Phys. Rev. A **93**, 033809 (2016)
11. J. Wiersig, Review of exceptional point-based sensors, Photonics Res. **8**, 1457 (2020)
12. J. Wiersig, Robustness of exceptional-point-based sensors against parametric noise: the role of Hamiltonian and Liouvillian degeneracies, Phys. Rev. A **101**, 053846 (2020)
13. A. Figotin, I. Vitebsky, Nonreciprocal magnetic photonic crystals, Phys. Rev. E **63**, 066609 (2001)
14. A. Figotin, I. Vitebskiy, Oblique frozen modes in periodic layered media, Phys. Rev. E **68**, 036609 (2003)
15. A. Figotin, I. Vitebskiy, Gigantic transmission band-edge resonance in periodic stacks of anisotropic layers, Phys. Rev. E **72**, 036619 (2005)
16. A. Figotin, I. Vitebskiy, Slow-wave resonance in periodic stacks of anisotropic layers, Phys. Rev. A **76**, 053839 (2007)
17. M.V. Berry, Physics of nonhermitian degeneracies, Czechoslovak J. Phys. **54**, 1039 (2004)
18. J. Wiersig, Prospects and fundamental limits in exceptional point-based sensing, Nat. Commun. **11**, 2454 (2020)
19. Y.-H. Lai, Y.-K. Lu, M.-G. Suh, Z. Yuan, K. Vahala, Observation of the exceptional-point-enhanced Sagnac effect, Nature **576**, 65 (2019)
20. W. Chen, S. Kaya Özdemir, G. Zhao, J. Wiersig, L. Yang, Exceptional points enhance sensing in an optical microcavity, Nature **548**, 192 (2017)
21. H.-K. Lau, A.A. Clerk, Fundamental limits and non-reciprocal approaches in non-Hermitian quantum sensing, Nat. Commun. **9**, 4320 (2018)
22. W. Langbein, No exceptional precision of exceptional-point sensors, Phys. Rev. A **98**, 023805 (2018)
23. M. Zhang, W. Sweeney, C.W. Hsu, L. Yang, A.D. Stone, L. Jiang, Quantum noise theory of exceptional point amplifying sensors, Phys. Rev. Lett. **123**, 180501 (2019)
24. C. Chen, L. Jin, R.-B. Liu, Sensitivity of parameter estimation near the exceptional point of a non-Hermitian system, New J. Phys. **21**, 083002 (2019)
25. M.Y. Nada, M.A.K. Othman, F. Capolino, Theory of coupled resonator optical waveguides exhibiting high-order exceptional points of degeneracy, Phys. Rev. B **96**, 184304 (2017)
26. A.F. Abdelshafy, M.A.K. Othman, D. Oshmarin, A.T. Almutawa, F. Capolino, Exceptional points of degeneracy in periodic coupled waveguides and the interplay of gain and radiation loss: theoretical and experimental demonstration, IEEE Trans. Antennas Propag. **67**, 6909 (2019)
27. H. Kazemi, M.Y. Nada, A. Nikzamir, F. Maddaleno, F. Capolino, Experimental Demonstration of Exceptional Points of Degeneracy in Linear Time Periodic Systems and Exceptional Sensitivity, arXiv:1908.08516 (2019)
28. H. Kazemi, M.Y. Nada, T. Mealy, A.F. Abdelshafy, F. Capolino, Exceptional points of degeneracy induced by linear time-periodic variation, Phys. Rev. Appl. **11**, 014007 (2019)
29. C.M. Bender, S. Boettcher, Real spectra in Non-Hermitian Hamiltonians having PT symmetry, Phys. Rev. Lett. **80**, 5243 (1998)
30. J. Schindler, A. Li, M.C. Zheng, F.M. Ellis, T. Kottos, Experimental study of active LRC circuits with PT symmetries, Phys. Rev. A **84**, 040101 (2011)
31. T. Stehmann, W.D. Heiss, F.G. Scholtz, Observation of exceptional points in electronic circuits, J. Phys. A **37**, 7813 (2004)
32. P.-Y. Chen et al., Generalized parity–time symmetry condition for enhanced sensor telemetry, Nat. Electr. **1**, 297 (2018)
33. K. Rouhi, R. Marosi, T. Mealy, A.F. Abdelshafy, A. Figotin, F. Capolino, Exceptional degeneracies in traveling wave tubes with dispersive slow-wave structure including space-charge effect, Appl. Phys. Lett. **118**, 263506 (2021)
34. A. Figotin, Exceptional points of degeneracy in traveling wave tubes, J. Math. Phys. **62**, 082701 (2021)
35. P. Djorwe, Y. Pennec, B. Djafari-Rouhani, Exceptional point enhances sensitivity of optomechanical mass sensors, Phys. Rev. Appl. **12**, 024002 (2019)
36. J. Ren et al., Ultrasensitive micro-scale parity-time-symmetric ring laser gyroscope, Opt. Lett. **42**, 1556 (2017)
37. B.D.H. Tellegen, The gyrator, a new electric network element, Philips Res. Rep. **3**, 81 (1948)
38. D.F. Sheahan, H.J. Orchard, Integratable gyrator using M.O.S. and bipolar transistors, Electr. Lett. **2**, 390 (1966)
39. T. Yanagisawa, Y. Kawashima, Active gyrator, Electr. Lett. **3**, 105 (1967)
40. H.T. Chua, R.W. Newcomb, Integrated direct-coupled gyrator, Electr. Lett. **3**, 182 (1967)

41. H. Th. van Looij, K.M. Adams, Wideband electronic gyrator circuit, Electr. Lett. **4**, 431 (1968)
42. D.F. Sheahan, H.J. Orchard, High-quality transistorised gyrator, Electr. Lett. **2**, 274 (1966)
43. T.N. Rao, R.W. Newcomb, Direct-coupled gyrator suitable for integrated circuits and time variation, Electr. Lett. **2**, 250 (1966)
44. W.H. Holmes, S. Gruetzmann, W.E. Heinlein, High-performance direct-coupled gyrators, Electr. Lett. **3**, 45 (1967)
45. B. Shenoi, Practical realization of a gyrator circuit and RC-gyrator filters, IEEE Trans. Circ. Theory **12**, 374 (1965)
46. A. Antoniou, Gyrators using operational amplifiers, Electr. Lett. **3**, 350 (1967)
47. A. Antoniou, New gyrator circuits obtained by using nullors, Electr. Lett. **4**, 87 (1968)
48. A. Antoniou, 3-terminal gyrator circuits using operational amplifiers, Electr. Lett. **4**, 591 (1968)
49. H.J. Orchard, A.N. Willson, New active-gyrator circuit, Electr. Lett. **10**, 261 (1974)
50. A. Antoniou, Realisation of gyrators using operational amplifiers, and their use in RC-active-network synthesis, Proc. Inst. Electr. Eng. **116**, 1838 (1969)
51. A. Morse, L. Huelsman, A gyrator realization using operational amplifiers, IEEE Trans. Circ. Theory **11**, 277 (1964)
52. A. Antoniou, K. Naidu, A compensation technique for a gyrator and its use in the design of a channel-bank filter, IEEE Trans. Circ. Syst. **22**, 316 (1975)
53. A. Antoniou, K. Naidu, Modeling of a gyrator circuit, IEEE Trans. Circ. Theory **20**, 533 (1973)
54. R.Y. Barazarte, G.G. Gonzalez, M. Ehsani, Generalized gyrator theory, IEEE Trans. Power Electr. **25**, 1832 (2010)
55. A. Figotin, Synthesis of lossless electric circuits based on prescribed Jordan forms, J. Math. Phys. **61**, 122703 (2020)
56. A. Figotin, Perturbations of circuit evolution matrices with Jordan blocks, J. Math. Phys. **62**, 042703 (2021)
57. K. Rouhi, A. Nikzamir, A. Figotin, F. Capolino, Enhanced Sensitivity of Degenerate System Made of Two Unstable Resonators Coupled by Gyrator Operating at an Exceptional Point, arXiv:2110.01860 (2021)
58. A. Nikzamir, K. Rouhi, A. Figotin, F. Capolino, Demonstration of Exceptional Points of Degeneracy in Gyrator-Based Circuit for High-Sensitivity Applications, arXiv:2107.00639 (2021)
59. A. Nikzamir, K. Rouhi, A. Figotin, F. Capolino, Exceptional points of degeneracy in gyrator-based coupled resonator circuit, in *2021 Fifteenth International Congress on Artificial Materials for Novel Wave Phenomena (Metamaterials)* (2021), pp. 302–304
60. K. Rouhi, H. Kazemi, A. Figotin, F. Capolino, Exceptional points of degeneracy directly induced by space-time modulation of a single transmission line, IEEE Antennas Wireless Propag. Lett. **19**, 1906 (2020)
61. A. Willson, H. Orchard, Realization of ideal gyrators, IEEE Trans. Circ. Syst. **21**, 729 (1974)
62. C.L. Hogan, The ferromagnetic faraday effect at microwave frequencies and its applications, Rev. Mod. Phys. **25**, 253 (1953)
63. C.L. Hogan, The ferromagnetic faraday effect at microwave frequencies and its applications, Bell Syst. Tech. J. **31**, 1 (1952)
64. Q. Zhang, T. Guo, B.A. Khan, T. Kodera, C. Caloz, Coupling matrix synthesis of nonreciprocal lossless two-port networks using gyrators and inverters, IEEE Trans. Microw. Theory Tech. **63**, 2782 (2015)
65. T. Kodera, D.L. Sounas, C. Caloz, Magnetless Nonreciprocal Metamaterial (MNM) technology: application to microwave components, IEEE Trans. Microw. Theory Tech. **61**, 1030 (2013)
66. A. Toker, O. Cicekoglu, H. Kuntman, New active gyrator circuit suitable for frequency-dependent negative resistor implementation, Microelectr. J. **30**, 59 (1999)
67. M. Ehsani, I. Husain, M.O. Bilgic, Power converters as natural gyrators, IEEE Trans. Circ. Syst. I **40**, 946 (1993)
68. I.M. Filanovsky, Current conveyor, voltage conveyor, gyrator, in *Proceedings of the 44th IEEE 2001 Midwest Symposium on Circuits and Systems. MWSCAS 2001 (Cat. No. 01CH37257)* (2001), pp. 314–317
69. A. Welters, On explicit recursive formulas in the spectral perturbation analysis of a Jordan block, SIAM J. Matrix Anal. Appl. **32**, 1 (2011)

Cite this article as: Kasra Rouhi, Alireza Nikzamir, Alexander Figotin, Filippo Capolino, High-sensitivity in various gyrator-based circuits with exceptional points of degeneracy, EPJ Appl. Metamat. **9**, 8 (2022)